

Discovery of Nuclear Water Maser Emission in Centaurus A

Jürgen Ott

National Radio Astronomy Observatory, P.O. Box O, 1003 Lopezville Road, Socorro, NM
87801, USA

jott@nrao.edu

David S. Meier

New Mexico Institute of Mining and Technology, 801 Leroy Place, Socorro, NM 87801, USA
National Radio Astronomy Observatory, P.O. Box O, 1003 Lopezville Road, Socorro, NM
87801, USA

dmeier@nmt.edu

Mark McCoy

New Mexico Institute of Mining and Technology, 801 Leroy Place, Socorro, NM 87801, USA

mmccoy@nmt.edu

Alison Peck

National Radio Astronomy Observatory, 520 Edgemont Road, Charlottesville, VA 22903,
USA

apecck@nrao.edu

Violette Impellizzeri

Joint ALMA Observatory, Alonso de Córdova 3107, Vitacura 763 0355, Santiago de Chile,
Chile

National Radio Astronomy Observatory, 520 Edgemont Road, Charlottesville, VA 22903,
USA

– 2 –

`vimpelli@alma.cl`

Andreas Brunthaler

Max-Planck Institute für Radioastronomie, Auf dem Hügel 69, 53121 Bonn, Germany

`brunthal@mpifr-bonn.mpg.de`

Fabian Walter

Max-Planck Institut für Astronomie, Königstuhl 17, 69117, Heidelberg, Germany

National Radio Astronomy Observatory, P.O. Box O, 1003 Lopezville Road, Socorro, NM
87801, USA

`walter@mpia.de`

Philip Edwards

CSIRO Astronomy and Space Science, PO Box 76, Epping NSW 1710, Australia

`Phil.Edwards@csiro.au`

Crystal N. Anderson

New Mexico Institute of Mining and Technology, 801 Leroy Place, Socorro, NM 87801, USA

`canderso@nmt.edu`

Christian Henkel

Max-Planck Institute für Radioastronomie, Auf dem Hügel 69, 53121 Bonn, Germany
Astronomy Department, Faculty of Science, King Abdulaziz University, P.O. Box 80203,
Jeddah, Saudi Arabia

`chenkel@mpifr-bonn.mpg.de`

Ilana Feain

CSIRO Astronomy and Space Science, PO Box 76, Epping NSW 1710, Australia

`Ilana.Feain@csiro.au`

and

Minnie Y. Mao

National Radio Astronomy Observatory, P.O. Box O, 1003 Lopezville Road, Socorro, NM
87801, USA

`mmao@nrao.edu`

Received _____; accepted _____

ABSTRACT

We report the detection of a 22 GHz water maser line in the nearest ($D \sim 3.8$ Mpc) radio galaxy Centaurus A using the Australia Telescope Compact Array (ATCA). The line is centered at a velocity of ~ 960 km s $^{-1}$, which is redshifted by about 400 km s $^{-1}$ from the systemic velocity. Such an offset, as well as the width of ~ 120 km s $^{-1}$, could be consistent with either a nuclear maser arising from an accretion disk of the central supermassive black hole, or for a jet maser that is emitted from the material that is shocked near the base of the jet in Centaurus A. The best spatial resolution of our ATCA data constrains the origin of the maser feature within < 3 pc from the supermassive black hole. The maser exhibits a luminosity of $\sim 1 L_{\odot}$, which classifies it as a kilomaser, and appears to be variable on timescales of months. A kilomaser can also be emitted by shocked gas in star forming regions. Given the small projected distance from the core, the large offset from systemic velocity, as well as the smoothness of the line feature, we conclude that a jet maser line emitted by shocked gas around the base of the AGN is the most likely explanation. For this scenario we can infer a minimum density of the radio jet of $\gtrsim 10$ cm $^{-3}$, which indicates substantial mass entrainment of surrounding gas into the propagating jet material.

Subject headings: masers, galaxies: individual (Centaurus A; NGC5128), ISM: jets and outflows

Centaurus A

1. Introduction

Centaurus A (Cen A) is by far the most nearby radio galaxy and one of the brightest radio sources in the sky. Its proximity of only 3.8 Mpc (Harris et al. 2010) makes it a unique target for studies of supermassive black hole (SMBH) accretion, jet formation and acceleration, as well as the interaction of the jets and lobes with the interstellar and intergalactic media.

Centaurus A (see Israel 1998, for a review of the properties of Cen A) is embedded in the giant elliptical host NGC 5128. Unlike most other elliptical galaxies, NGC 5128 displays very prominent dust lanes that are likely due to merger activity in the past (see e.g. Israel 1998; Barnes 2002; Auld et al. 2012, and references therein). NGC 5128 may thus be in the process of rebuilding a strongly warped, gaseous disk (e.g. Quillen et al. 2006; Neumayer et al. 2007; Struve et al. 2010; Quillen et al. 2010), which shows signatures of spiral arms (Espada et al. 2012). These properties may affect the gas accretion process onto the active SMBH (mass: $\sim 5.5 \times 10^7 M_{\odot}$; Cappellari et al. 2009).

22 GHz water (H_2O) masers have proven to be great tools to study the environment close to SMBHs. Water masers are collisionally pumped (e.g. Kylafis & Norman 1991) and the requisite high gas densities are typically achieved in shock fronts. Thus, H_2O masers can be found in very diverse environments. Typical locations include shells of expanding asymptotic giant branch stars, expanding envelopes of young stellar objects, accretion disks of SMBHs and interaction zones of radio jets with the surrounding media (see Lo 2005, for a review). The latter two are often referred to as ‘disk masers’ (e.g. Greenhill et al. 1995; Lo 2005) and ‘jet masers’ (e.g. Claussen et al. 1998; Peck et al. 2003). Studying nearby jet

and disk masers may also lead to a better understanding of SMBHs in the high redshift regime. Due to their brightness, 22 GHz water masers have been observed up to $z \sim 2.64$ (Impellizzeri et al. 2008; Castangia et al. 2011).

In the past, Cen A was target of a number of unsuccessful H_2O maser emission searches (e.g. Claussen & Lo 1986; Braatz et al. 1996, 2004; Surcis et al. 2009). In the following, we report the first detection of a water maser toward the nuclear environment of Cen A. Our observations and data reduction steps are described in § 2, followed by a presentation of our results in § 3, and a discussion on the nature of the detected maser feature in § 4. We summarize our findings in § 5.

2. Observations and Data Reduction

We observed Cen A with the Australia Telescope Compact Array (ATCA). The ATCA is a 6 antenna interferometer with baselines between 30 m and 6 km. The observations were performed around the rest frequency of the $J = 6_{16} - 5_{23}$ water transition at 22.23508 GHz. To exclude cross-identification of instrumental features with the water line, we slightly shifted the central frequencies between some of the observations (see Table 1). We used the Compact Array Broadband Backend (CABB; Wilson et al. 2011) in two different modes: A wideband mode, with a total bandwidth of two times 1 GHz and a channel width of 1 MHz (or 13 km s^{-1} velocity resolution; CFB 1M-0.5k mode) and CFB 64M-32k, where we tuned one of the 64 MHz wide zooms to water (total velocity range of $\sim 860 \text{ km s}^{-1}$; channel width of 23 kHz or 0.4 km s^{-1}). To reduce systematic effects, we observed at different central frequencies (see Table 1). After cropping bandpass edges, the velocity range of the narrow band observations amounts to $\sim 620 - 1380 \text{ km s}^{-1}$ for a central frequency of 22.172 GHz and $\sim 440 - 1290 \text{ km s}^{-1}$ for 22.272 GHz. Absolute fluxes were calibrated with the ATCA standard PKS 1934-638. Bandpasses were typically obtained by observing PKS 1253-055

for ~ 15 min, but we used PKS 0537-441 when the former was not available at the start of the observations. The observational setups and properties are summarized in Table 1, where we list the dates of the observations in column (1), the ATCA array configurations in column (2), the central frequencies and bandwidths of the instrumental setups in columns (3) and (4), the beam sizes and position angles in columns (5) and (6), the continuum fluxes in column (7), and the rms noise values, the channel separations, and the on-source integration times in columns (8), (9), and (10), respectively.

The data were self-calibrated on the strong continuum emission from the core of Cen A to correct phase and gain variations as a function of time. Finally, we extracted spectra from the images, after robust weighting and cleaning 1000 iterations per channel. All data reduction steps were performed in MIRIAD. Whereas the narrowband observations show sufficiently flat baselines, fitted well by 0th order polynomials, the wideband observations exhibit variations of order $\sim 1 - 2$ per cent. Given the relatively high flux density of the central source (see Table 1) these variations amount to a ~ 100 mJy level, and we fitted and subtracted third order polynomials to a ~ 2000 km s $^{-1}$ range around the water frequency for satisfactory results. Given the spectral variations of the baselines, we estimate ~ 10 per cent uncertainty for the absolute fluxes of the well behaved narrowband observations, and a conservative ~ 15 per cent error for the wideband data.

3. Results

We extracted line emission at the central position of the SMBH at RA(J2000)= $13^h25^m27.6$, DEC(J2000)= $-43^\circ01'09''$ and subtracted the continuum emission. The wideband spectra are shown in Fig. 1 and the narrowband data in Fig. 2. The systemic velocity of Cen A is at a kinematic Local Standard of Rest (LSRK) value of ~ 545 km s $^{-1}$ (Saviane & Jerjen 2007) and we mark this value in the figures, assuming that the line can be identified

as the $J = 6_{16} - 5_{23}$ water maser transition at a rest frequency of 22.23508 GHz (see §4.2). We clearly detect a spatially unresolved emission feature at $\sim 950 \text{ km s}^{-1}$ offset from systemic. No detections are seen at systemic and blueshifted velocities. As the narrowband observations resulted in higher quality spectra, we used these data to constrain the line properties. Although the lines do not appear to be perfectly Gaussian in shape, we nevertheless fitted one-component Gaussians to these lines. The results are listed in Table 2 and plotted in Fig. 2. The table contains the dates of the observations in column (1), followed by the best fit central LSRK velocities v_c , the full widths at half maximum of the fitted line v_{FWHM} and the peak fluxes S_p in columns (2), (3), and (4). In column (5) we list the derived isotropic luminosity values in L_{\odot} . The resulting parameters reveal that the H_2O maser line is at a velocity of $\sim 960 \text{ km s}^{-1}$ redshifted $\sim 415 \text{ km s}^{-1}$ from systemic, with a width of $\sim 120 \text{ km s}^{-1}$. The amplitude is $\sim 20 \text{ mJy}$ with the exception of the data taken on 2012 May 22, where we find a three times higher peak flux density of $\sim 60 \text{ mJy}$. The continuum flux at this epoch is only about 30 per cent higher than the lowest measured continuum flux at all epochs, whereas the line is ~ 3 times stronger. Although some continuum variations could be due to the different synthesized beam sizes of the individual observations (see Table 1), this suggests that the variation is predominantly intrinsic to Cen A.

4. Discussion

4.1. Location of the Line Emission

Our observations are consistent with unresolved line emission emerging from the center of Cen A. For each of the 6 km array data, the beams (see Table 1) correspond to physical resolutions of about $14.6 \text{ pc} \times 5.9 \text{ pc}$ and $22.7 \text{ pc} \times 6.6 \text{ pc}$. The position angles of the two observations are separated by $\sim 40^\circ$, and we can assume that the line is emitted from

within the overlap region with a conservative upper limit of a maximum of < 3 pc projected distance away from the SMBH.

4.2. Line Identification

We observe the line feature at a sky frequency of ~ 22.162 MHz. If the line would originate in Cen A at its systemic velocity of 545 km s^{-1} LSRK, the line rest frequency would be expected to be close to a value of ~ 22.202 MHz. Adding a potential velocity offset of $\pm 1000 \text{ km s}^{-1}$ (or ± 75 MHz), the following astrophysical spectral lines other than the H_2O $J = 6_{16} - 5_{23}$ maser transition with a rest frequency of 22.23508 GHz may be candidates for the emission in Cen A¹: CH_2OHCHO $J = 4_{13} - 4_{04}$ at a rest frequency of 22.143 MHz, C^{13}CS $J = 1_2 - 0_1$ at ~ 22.255 GHz, and CCO $J = 1_2 - 0_1$ at 22.258 GHz. None of these lines are expected to be bright enough to explain the observed intensity. And none of them lie near systemic velocity requiring very unusual kinematics if they are within a star forming cloud that is at a projected distance no further than 3 pc from the core of Cen A (§4.1). In addition, given the strong continuum of Cen A, all of the thermal lines are more likely to be detectable in absorption and not emission (Cen A has a complex molecular absorption spectrum as, e.g., shown in Eckart et al. 1990; Israel 1992; Wiklind & Combes 1997; Israel 1998; Muller & Dinh-V-Trung 2009; Espada et al. 2010). Apart from the molecules, the $\text{H}83\beta$ radio recombination line has a rest frequency of 22.196 GHz and could be a potential candidate for the emission. But given that we do not even see any $\text{H}\alpha$ recombination lines in our spectra, we can exclude an identification with the much weaker $\text{H}\beta$ line. The only likely line candidate is the redshifted H_2O maser $J = 6_{16} - 5_{23}$ transition, which is by far the brightest astrophysical transition across the observed frequency range. As alluded to

¹as taken from the Lovas catalogue: <http://physics.nist.gov/cgi-bin/micro/table5/start.pl>

in the introduction (§1), H_2O has also been observed toward the nuclei of other active galaxies, and the maser line is the most likely one observed in emission in the presence of Cen A’s strong continuum emission.

4.3. Maser strength

The maser feature has a FWHM of $\sim 120 \text{ km s}^{-1}$, which we cannot decompose into more narrow individual maser features down to our $\sim 1 \text{ km s}^{-1}$ velocity resolution. We may thus assume that the line emerges from a single maser spot unless high resolution imaging will break it up into more components. The isotropic luminosity of the feature is $\sim 1 L_\odot$ (see Table 2). If the maser line is emitted from a single spot, it falls into the category of kilomasers. H_2O masers of similar strengths are found in nearby, moderately star forming galaxies and mergers such as M 51, NGC 253, M 82, NGC 2146, NGC 3556, NGC 3620 or the Antennae (Claussen et al. 1984; Ho et al. 1987; Nakai & Kasuga 1988; Tarchi et al. 2002; Henkel et al. 2004; Lo 2005; Henkel et al. 2005; Surcis et al. 2009; Brunthaler et al. 2009; Brogan et al. 2010). It is also similar to the Galaxy’s most luminous water maser in W49N (e.g. Walker et al. 1982).

In all but one epoch the peak of the maser feature is about 20 mJy. The 2012 May 22 data, however, reveal a three times stronger line (see §3). The variability may be related to a merely ~ 30 per cent stronger continuum flux at the time, which may indicate that the maser itself is unsaturated. To determine this conclusively, however, requires more epochs of observations, desirably at higher spatial resolution.

4.4. Star Formation, Jet, or Disk Maser?

Most kilomasers are found in star formation regions of galaxies (see references above and, e.g. Baudry & Brouillet 1996). They typically arise from outflows of massive stars and show velocity spreads of up to a few tens of km s^{-1} . For Cen A, we can pinpoint the maser to within $< 3 \text{ pc}$ projected distance from the nucleus (§ 4.1). We consider the probability of crossing a massive star formation region along the line of sight to be low. Even if such a region is located toward that direction, the velocity offset of $\sim 400 \text{ km s}^{-1}$ from systemic and the linewidth of $\sim 120 \text{ km s}^{-1}$ would be inconsistent with a typical H_2O maser in a star forming region well outside the nuclear region.

Strong water masers are also observed toward the accretion disks of some SMBHs (“disk masers”) and close to AGN jet-ISM interaction regions (“jet masers”). Typical examples for disk masers are the archetypical NGC 4258 galaxy (e.g. Greenhill et al. 1995; Lo 2005) and a larger sample of such masers have been observed in dedicated search campaigns (e.g. Tarchi et al. 2002; Henkel et al. 2005; Kondratko et al. 2006; Braatz & Gugliucci 2008; Castangia et al. 2008; Bennert et al. 2009; Surcis et al. 2009; König et al. 2012). Disk masers typically have three main components: one at systemic velocity as well as blueshifted and redshifted line features, both offset by a few hundred km s^{-1} . Some disks, however, lack one or two of these main components. At high velocity resolution (see, e.g. Braatz & Gugliucci 2008) the disk maser components show significant substructures at km s^{-1} linewidth scales. They can overlap and blend to form broader components. Although we may see some indications of substructure in the wideband data that was observed in 2011 (see Fig. 1), the overall H_2O spectrum in Cen A is relatively smooth, even at the km s^{-1} scales of our high spectral resolution data (Fig. 2). We thus consider a disk maser origin unlikely.

Jet masers, have been detected in NGC 1068 (Gallimore et al. 1996), NGC 3079

(Trotter et al. 1998), Circinus (Greenhill et al. 2003), Mrk 348 (Peck et al. 2003) and possibly in NGC 1052 (Claussen et al. 1998; Kamenno et al. 2005). In particular, the jet maser in Mrk 348 resembles Cen A’s maser in many respects. The line is $\sim 130 \text{ km s}^{-1}$ redshifted from systemic, 130 km s^{-1} wide and relatively smooth. Very Long Baseline Array data shows that the maser is about $\sim 1 \text{ pc}$ away from the core. Monitoring also shows some significant variability on timescales as short as a day and loosely correlated with the continuum strength (Peck et al. 2003). The isotropic luminosity of the Mrk 348 maser, however, is about two orders of magnitude higher than the feature in Cen A. We also observe similarities with the possible jet maser in NGC 1052. The H_2O line in NGC 1052 is redshifted $\sim 400 \text{ km s}^{-1}$ from systemic with a linewidth of $\sim 200 \text{ km s}^{-1}$. Its isotropic luminosity is of the same order as the maser in Mrk 348. Given the similarities of the Cen A H_2O maser emission with the above cases, we discuss the implications of the jet maser model for Cen A in the following section.

4.5. Jet Maser Properties

A useful model for a jet maser has been established by Peck et al. (2003). They propose that the jet plows into a neighboring molecular cloud and creates a shock front that is propagating away from the jet direction. The tip of the shock front covers a large opening angle, and the morphology resembles that of a mushroom, with cloud material being compressed toward the front and the the sides of the jet. The projected velocities of the shocked material may thus combine to the large linewidth that we witness. Shocks propagate according to the density contrast between the the two media at the shock boundary via $\rho_i v_i^2 = \rho_o v_o^2$, where ρ_i and v_i are the density and velocity of the initial, shocking material and ρ_o and v_o of the propagating forward shock front in the material that was hit. Tingay et al. (1998) monitored the motions of the parsec-scale jet components in

Cen A and derived velocities of $v_i \sim 0.1c$. For a shock that propagates with the velocity offset of the maser feature in Cen A, $v_o \sim 400 \text{ km s}^{-1}$, we can then derive a density contrast of $\sim 2 \times 10^{-4}$. Interstellar H_2O masers require volume densities of at least $> 10^7 \text{ cm}^{-3}$ (Yates et al. 1997; Lo 2005) to be pumped (see Kylafis & Norman 1991, for scenarios when radiative pumping may become important). When we apply the density contrast to this number we can infer an incoming jet density of $> 10^3 \text{ cm}^{-3}$. Geometry constraints will change the numbers but the order of magnitude estimate should remain if the shock front has a large opening angle as suggested by Peck et al. (2003). The jet velocity, however, may be underestimated. Tingay et al. (1998) shows that the northern jet is much brighter than the southern counterpart, which can be explained by Doppler boosting the brightness of the approaching jet. Such an effect would be expected at much higher velocities than the $\sim 0.1c$ measured for the individual components. For the limit of a jet velocity at light speed the above calculations will reduce the lower limit of the jet density by two orders of magnitude and we thus estimate a more conservative $\rho_i > 10 \text{ cm}^{-3}$. But even such a reduced value is much larger than typical electron-positron or thermal gas plasma densities expected for relativistic jets. The radio galaxy 3C120, for example, has densities $\lesssim 10^{-3} \text{ cm}^{-3}$ (Walker et al. 1987), which is four orders of magnitude lower than our limit for the jet of Cen A. The difference can potentially be explained by surrounding material that is evaporated by and entrained into the jet during its outward propagation.

Kameno et al. (2005) find indications for the appearance of narrow components in the otherwise broad maser spectrum of NGC1052. These components show flux variabilities and line narrowing on timescales of days. Our 2011 ATCA broadband H_2O spectra of Cen A show indications for similar, transient narrow features. In the jet maser model such variations could be due to the jet shocking small, high density substructures of the molecular cloud. The maser properties could be the response to the shock dynamics that includes local density enhancements competing with H_2O shock dissociation.

The Cen A maser line is redshifted to velocities larger than systemic. The receding, fainter jet may thus be a natural location for the origin of the jet maser feature. We note, however, that Very Long Baseline Array data show that the similarly redshifted H_2O maser in Mrk 348 originates from the approaching, brighter jet component of this galaxy. The full location and geometry of the maser spots in Cen A are therefore uncertain until higher resolution imaging will be available.

5. Summary

We report the detection of a 22 GHz $J = 6_{16} - 5_{23}$ water maser emission line toward the inner 3 pc of the most nearby radio galaxy Centaurus A. The weak and slightly variable maser feature can be classified as a kilomaser and could have its origin in a star formation region, a nuclear disk around the central supermassive black hole, or from material that is shocked close to the jet base of Cen A. Given the relative smoothness and width of the line, as well as its central location, we conclude that the “jet maser” scenario is the most likely one. In this case, the radio jet is shocking a central molecular cloud. From the shock properties, a lower limit to the density of the jet of $> 10 \text{ cm}^{-3}$ can be derived. A full characterization of the nature and properties of the maser will require higher spatial resolution. The discovery of a nuclear water maser in Cen A opens up further opportunities to probe the extreme environments very close to a SMBH.

We thank the Australia Telescope National Facility staff for their assistance, and gratefully acknowledge the allocation of some Director’s Time to confirm this feature. This research has made use of NASA’s Astrophysics Data System and the NASA/IPAC Extragalactic Database (NED) which is operated by the Jet Propulsion Laboratory, California Institute of Technology, under contract with the National Aeronautics and Space

Administration.

Facilities: ATCA

REFERENCES

- Auld, R., Smith, M. W. L., Bendo, G., et al. 2012, MNRAS, 420, 1882
- Barnes, J. E. 2002, MNRAS, 333, 481
- Baudry, A., & Brouillet, N. 1996, A&A, 316, 188
- Bennert, N., Barvainis, R., Henkel, C., & Antonucci, R. 2009, ApJ, 695, 276
- Braatz, J. A., Wilson, A. S., & Henkel, C. 1996, ApJS, 106, 51
- Braatz, J. A., Henkel, C., Greenhill, L. J., Moran, J. M., & Wilson, A. S. 2004, ApJ, 617, L29
- Braatz, J. A., & Gugliucci, N. E. 2008, ApJ, 678, 96
- Brogan, C., Johnson, K., & Darling, J. 2010, ApJ, 716, L51
- Brunthaler, A., Castangia, P., Tarchi, A., et al. 2009, A&A, 497, 103
- Cappellari, M., Neumayer, N., Reunanen, J., et al. 2009, MNRAS, 394, 660
- Castangia, P., Tarchi, A., Henkel, C., & Menten, K. M. 2008, A&A, 479, 111
- Castangia, P., Impellizzeri, C. M. V., McKean, J. P., et al. 2011, A&A, 529, A150
- Claussen, M. J., Heiligman, G. M., & Lo, K. Y. 1984, Nature, 310, 298
- Claussen, M. J., & Lo, K.-Y. 1986, ApJ, 308, 592
- Claussen, M. J., Diamond, P. J., Braatz, J. A., Wilson, A. S., & Henkel, C. 1998, ApJ, 500, L129
- Eckart, A., Cameron, M., Genzel, R., et al. 1990, ApJ, 365, 522

- Espada, D., Peck, A. B., Matsushita, S., et al. 2010, *ApJ*, 720, 666
- Espada, D., Matsushita, S., Peck, A. B., et al. 2012, *ApJ*, 756, L10
- Gallimore, J. F., Baum, S. A., O’Dea, C. P., Brinks, E., & Pedlar, A. 1996, *ApJ*, 462, 740
- Greenhill, L. J., Jiang, D. R., Moran, J. M., et al. 1995, *ApJ*, 440, 619
- Greenhill, L. J., Booth, R. S., Ellingsen, S. P., et al. 2003, *ApJ*, 590, 162
- Harris, G. L. H., Rejkuba, M., & Harris, W. E. 2010, *PASA*, 27, 457
- Henkel, C., Tarchi, A., Menten, K. M., & Peck, A. B. 2004, *A&A*, 414, 117
- Henkel, C., Peck, A. B., Tarchi, A., et al. 2005, *A&A*, 436, 75
- Ho, P. T. P., Martin, R. N., Henkel, C., & Turner, J. L. 1987, *ApJ*, 320, 663
- Impellizzeri, C. M. V., McKean, J. P., Castangia, P., et al. 2008, *Nature*, 456, 927
- Israel, F. P. 1992, *A&A*, 265, 487
- Israel, F. P. 1998, *A&A Rev.*, 8, 237
- Kamenno, S., Nakai, N., Sawada-Satoh, S., Sato, N., & Haba, A. 2005, *ApJ*, 620, 145
- Kondratko, P. T., Greenhill, L. J., Moran, J. M., et al. 2006, *ApJ*, 638, 100
- König, S., Eckart, A., Henkel, C., & García-Marín, M. 2012, *MNRAS*, 420, 2263
- Kylafis, N. D., & Norman, C. A. 1991, *ApJ*, 373, 525
- Lo, K. Y. 2005, *ARA&A*, 43, 625
- Muller, S., & Dinh-V-Trung 2009, *ApJ*, 696, 176
- Nakai, N., & Kasuga, T. 1988, *PASJ*, 40, 139

- Neumayer, N., Cappellari, M., Reunanen, J., et al. 2007, *ApJ*, 671, 1329
- Peck, A. B., Henkel, C., Ulvestad, J. S., et al. 2003, *ApJ*, 590, 149
- Quillen, A. C., Brookes, M. H., Keene, J., et al. 2006, *ApJ*, 645, 1092
- Quillen, A. C., Neumayer, N., Oosterloo, T., & Espada, D. 2010, *PASA*, 27, 396
- Saviane, I., & Jerjen, H. 2007, *AJ*, 133, 1756
- Struve, C., Oosterloo, T. A., Morganti, R., & Saripalli, L. 2010, *A&A*, 515, A67
- Surcis, G., Tarchi, A., Henkel, C., et al. 2009, *A&A*, 502, 529
- Tarchi, A., Henkel, C., Peck, A. B., & Menten, K. M. 2002, *A&A*, 389, L39
- Tingay, S. J., Jauncey, D. L., Reynolds, J. E., et al. 1998, *AJ*, 115, 960
- Trotter, A. S., Greenhill, L. J., Moran, J. M., et al. 1998, *ApJ*, 495, 740
- Walker, R. C., Matsakis, D. N., & Garcia-Barreto, J. A. 1982, *ApJ*, 255, 128
- Walker, R. C., Benson, J. M., & Unwin, S. C. 1987, *ApJ*, 316, 546
- Wiklind, T., & Combes, F. 1997, *A&A*, 324, 51
- Wilson, W. E., Ferris, R. H., Axtens, P., et al. 2011, *MNRAS*, 416, 832
- Yates, J. A., Humphreys, E. M. L., & Richards, A. M. S. 1997, *Ap&SS*, 251, 285

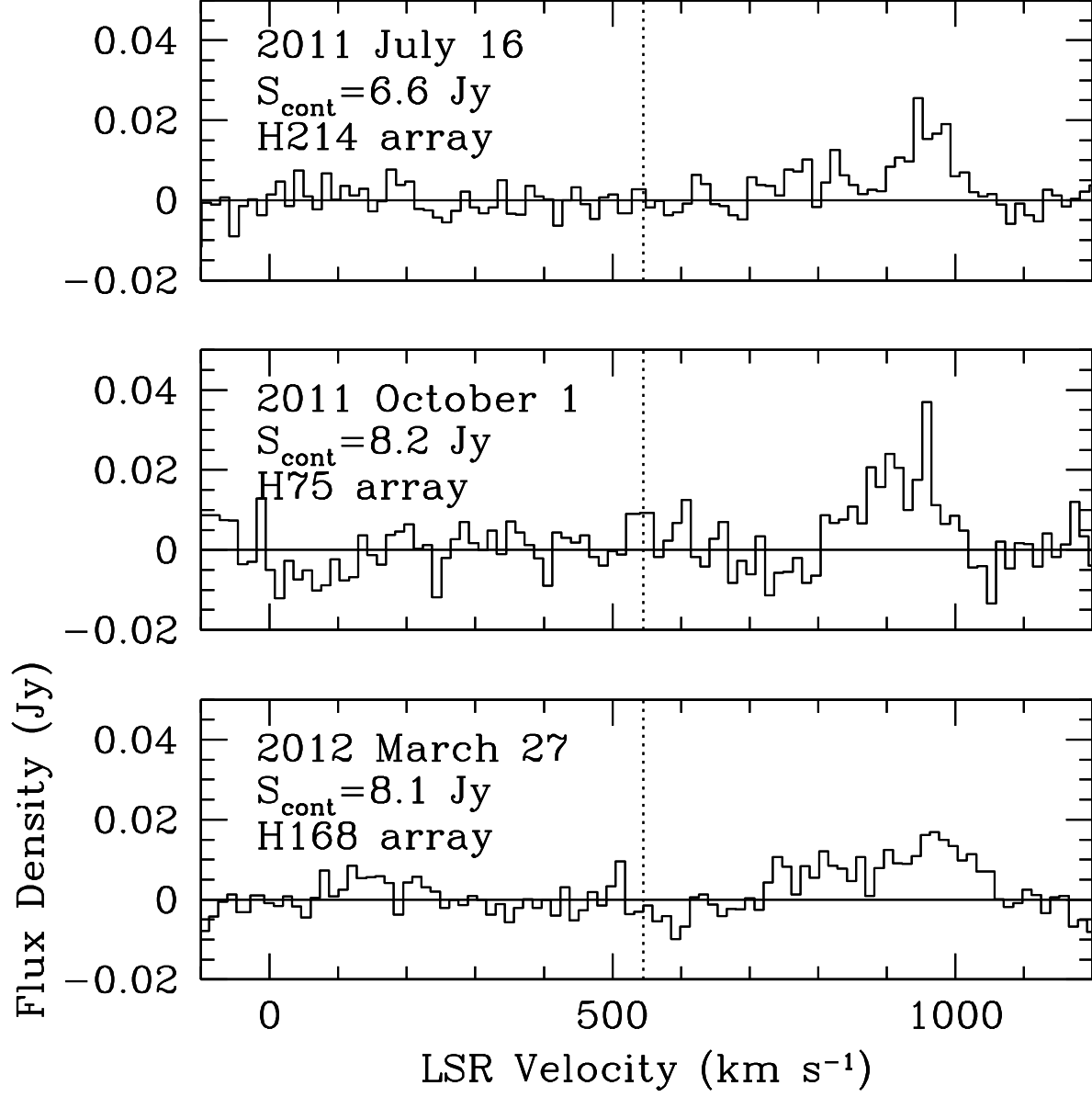


Fig. 1.— Spectra from three different epochs of ATCA observations in the broadband mode. The dashed vertical lines indicate the systemic velocity of NGC 5128 (545 km s^{-1} LSRK). The shown spectra cover the -100 km s^{-1} to 1200 km s^{-1} range of the full 1 GHz observations.

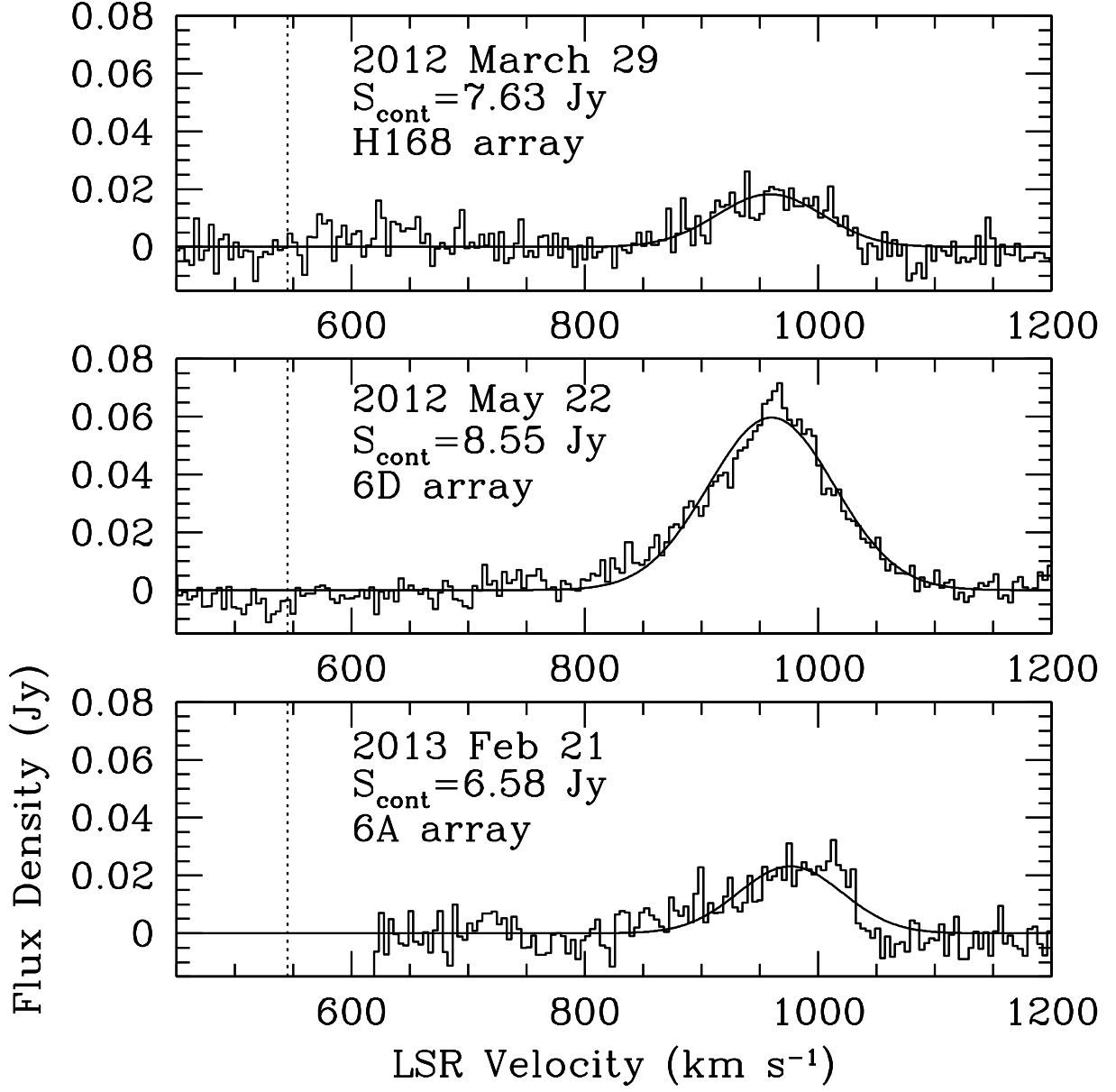


Fig. 2.— Narrowband spectra of the Cen A water maser line at three different epochs. The dashed vertical lines again indicate the systemic velocity of NGC 5128 (545 km s⁻¹ LSRK). The best fitting Gaussian is shown on top of each spectrum.

Table 1. Summary of the ATCA observations.

Date	Array	ν_{center} (GHz)	BW (MHz)	beam size ($''$)	Beam PA (deg)	S_{cont} (Jy)	rms (mJy beam $^{-1}$)	Δv (km s $^{-1}$)	t_{int} (h)
(1)	(2)	(3)	(4)	(5)	(6)	(7)	(8)	(9)	(10)
2011 July 16	H 214	22.450	1000	8.32 \times 6.59	82.3	6.6 \pm 1.0	10	13	8
2011 October 1	H 75	22.450	1000	26.80 \times 20.68	87.9	8.2 \pm 1.2	5	13	9
2012 March 27	H 168	22.494	1000	12.22 \times 8.84	82.7	8.1 \pm 1.2	4	13	8
2012 March 29	H 168	22.172	64	12.30 \times 9.46	77.5	7.63 \pm 0.76	3	0.4	10
2012 May 22	6 D	22.172	64	0.79 \times 0.32	18	8.66 \pm 0.87	6	0.4	8
2013 February 21	6 A	22.162	64	1.23 \times 0.36	-26.5	6.58 \pm 0.66	15	0.4	5.5

Table 2. Properties of the Gaussian fits to the narrowband spectra.

Date	v_c (LSRK) (km s $^{-1}$)	v_{FWHM} (km s $^{-1}$)	S_p (mJy)	L_{\odot}
(1)	(2)	(3)	(4)	(5)
2012 March 29	959 \pm 4	107 \pm 11	18.2 \pm 2.3	0.7 \pm 0.1
2012 May 22	960 \pm 1	127 \pm 3	59.8 \pm 6.1	2.7 \pm 0.3
2013 Feb 21	965 \pm 5	126 \pm 12	23.1 \pm 2.9	1.0 \pm 0.1